

Supplementary Information

**Cobalt Phosphide Supported by Two-Dimensional Molybdenum Carbide (MXene)
for Hydrogen Evolution Reaction, Oxygen Evolution Reaction, and Overall Water
Splitting**

Shilong Liu,^a Zongshan Lin,^a Rendian Wan,^a Yonggang Liu,^b Zhe Liu,^b Shuidong Zhang,^c

Xiaofeng Zhang,^d Zhenghua Tang,^{,b,c} Xiaoxing Lu,^{*,a} and Yong Tian^{*,a}*

^a School of Pharmacy, Guangdong Pharmaceutical University, Guangzhou, 510006, P. R. China. Emails: xxlu@gdpu.edu.cn, tian_yong_tian@163.com

^b Guangzhou Key Laboratory for Surface Chemistry of Energy Materials, New Energy Research Institute, School of Environment and Energy, South China University of Technology, Guangzhou Higher Education Mega Center, Guangzhou, Guangdong 510006, China. Email: zhht@scut.edu.cn

^c Guangdong Provincial Key Laboratory of Technique and Equipment for Macromolecular Advanced Manufacturing, South China University of Technology, China.

^d Institute of New Materials, Guangdong Academy of Science, Guangzhou, 510650, China.

List of Figures

Figure S1. SEM image of the MAX precursor.

Figure S2. SEM image of the Co(OH)F (a) and Co(OH)F/Mo₂CT_x (b) precursor.

Figure S3. XRD pattern of the Mo₂Ga₂C phase and the Mo₂C MXene phase.

Figure S4. XRD pattern of Co(OH)F/Mo₂CT_x.

Figure S5. High resolution XPS spectra of the Mo 3d (a) and C 1s (b) electrons for CoP/Mo₂CT_x.

Figure S6. N₂ adsorption-desorption isotherm of various catalysts.

Figure S7. Exchange current densities of the electrocatalysts.

Figure S8. Raman spectra of CoP/Mo₂CT_x before and after HER test.

Figure S9. (a) SEM and (b) TEM image of CoP/Mo₂CT_x after the stability test of HER.

Figure S10. (a) SEM and (b) TEM image of CoP/Mo₂CT_x after the stability test of OER.

Figure S11. Cyclic voltammograms of (a) Mo₂C MXene, (b) CoP, and (c) CoP/Mo₂CT_x in the region of 0-0.1 V in 1.0 M KOH at various scan rates and (d) the plots of current density as a function of scan rate derived from (a-c), respectively.

Figure S12. Cyclic voltammograms of (a) Mo₂C MXene, (b) CoP, and (c) CoP/Mo₂CT_x in the region of 1.02-1.12 V in 1.0 M KOH at various scan rates and (d) the plots of current density as a function of scan rate derived from (a-c), respectively.

Figure S13. The electrochemically active surface area of different catalysts in HER (a) and OER (b) test.

Figure S14. Mass activity for various catalysts in HER (a) and OER (b) test.

Figure S15. The calculation models of CoP (a), Mo₂C MXene (b), and CoP/Mo₂CT_x (c).

Figure S16. FTIR spectrum of CoP/Mo₂CT_x after OER test.

Figure S17. XRD patterns of CoP/Mo₂CT_x after OER test.

Figure S18. SEM image of CoP/Mo₂CT_x (fresh sample) and corresponding elemental mapping, EDX pattern with elemental composition of CoP/Mo₂CT_x.

Figure S19. SEM image of CoP/Mo₂CT_x (Post-OER sample) and corresponding elemental mapping, EDX pattern with elemental composition of CoP/Mo₂CT_x.

List of Tables

Table S1. The content of Co, P, and Mo elements percentage for all samples, measured by inductively coupled plasma-atomic emission spectroscopy (ICP-AES).

Table S2. Comparison of HER performance for non-precious metal electrocatalysts in 1.0 M KOH.

Table S3. Fitting parameters obtained from the EIS data for the HER in 1 M KOH.

Table S4. Comparison of OER performance for non-precious metal electrocatalysts in 1.0 M KOH.

Table S5. Fitting parameters obtained from the EIS data for the OER in 1 M KOH.

Table S6. Comparison of two electrode water splitting cell voltage of CoP/Mo₂CT_x with recently reported bifunctional electrocatalysts in alkaline medium.

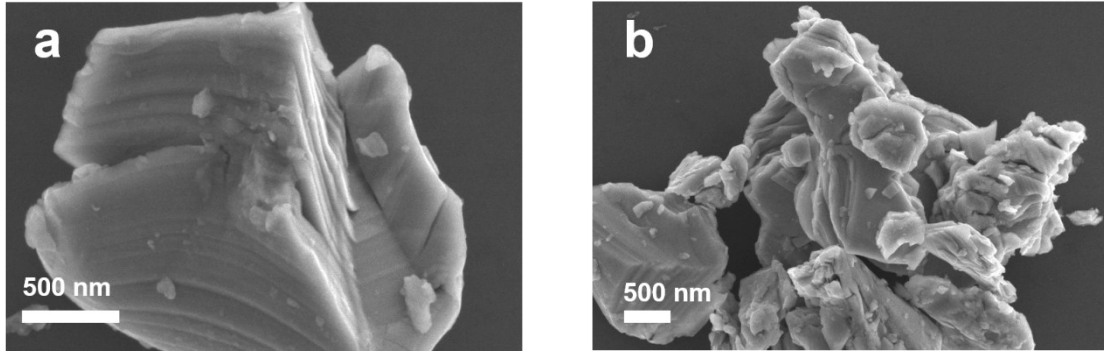


Figure S1. SEM image of the MAX precursor.

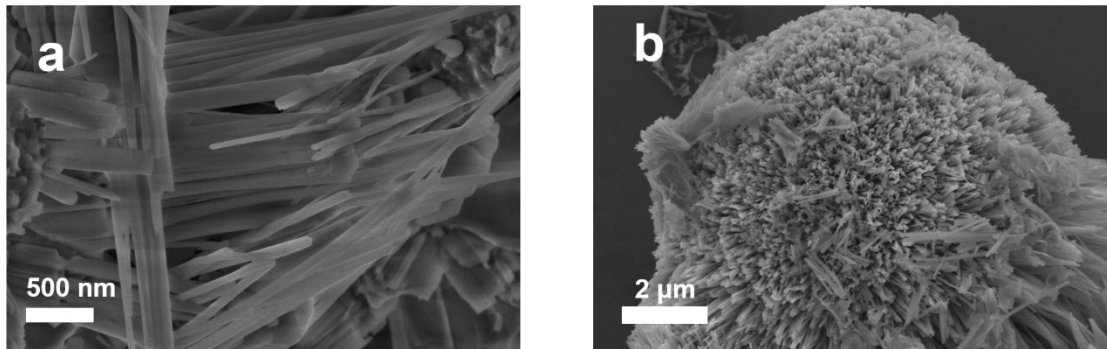


Figure S2. SEM image of the Co(OH)F (a) and Co(OH)F/Mo₂CT_x (b) precursor.

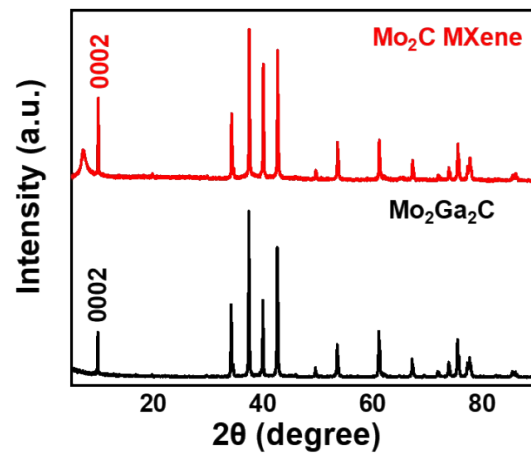


Figure S3. XRD pattern of the Mo₂Ga₂C phase and the Mo₂C MXene phase.

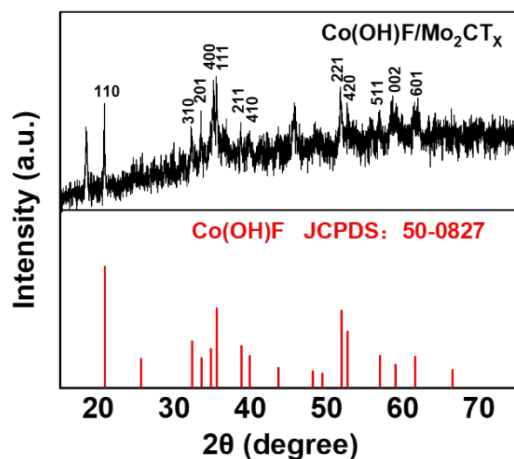


Figure S4. XRD pattern of $\text{Co(OH)F/Mo}_2\text{CT}_x$.

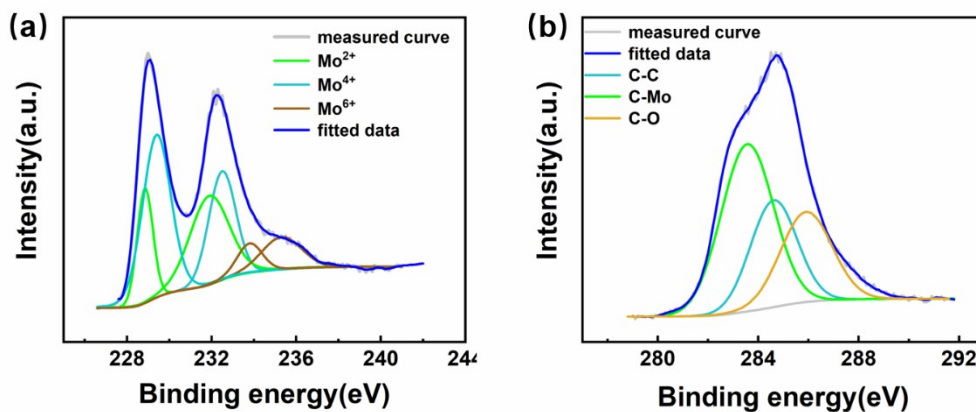


Figure S5. High resolution XPS spectra of the Mo 3d (a) and C 1s (b) electrons for $\text{CoP/Mo}_2\text{CT}_x$.

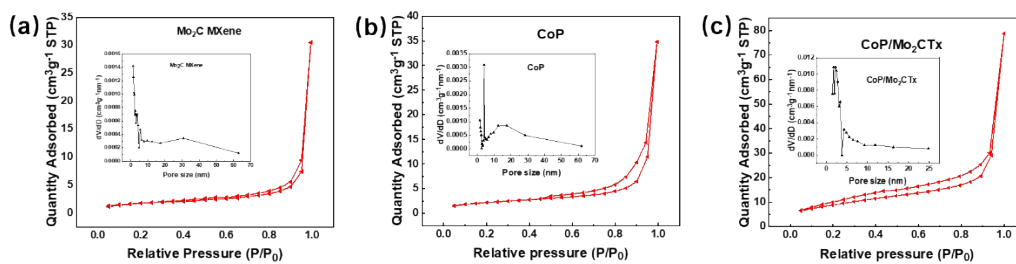


Figure S6. N_2 adsorption-desorption isotherm of various catalysts.

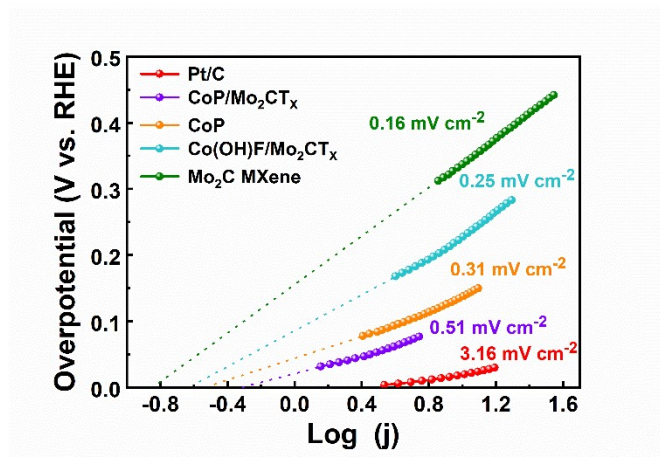


Figure S7. Exchange current densities of the electrocatalysts.

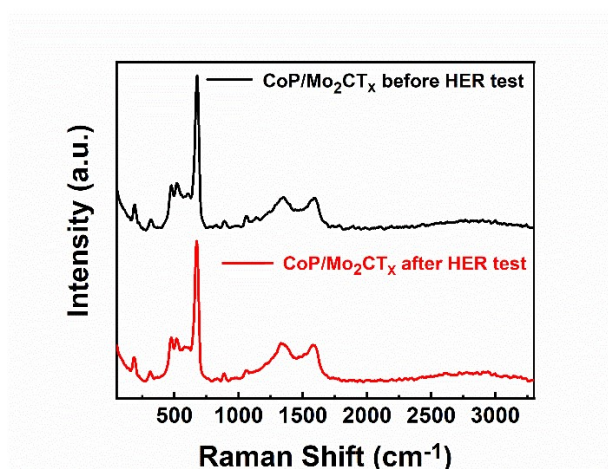


Figure S8. Raman spectra of CoP/Mo₂CT_x before and after HER test.

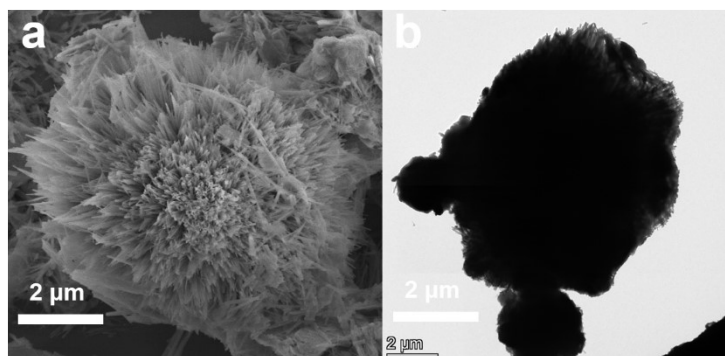


Figure S9. (a) SEM and (b) TEM image of CoP/Mo₂CT_x after the stability test of HER.

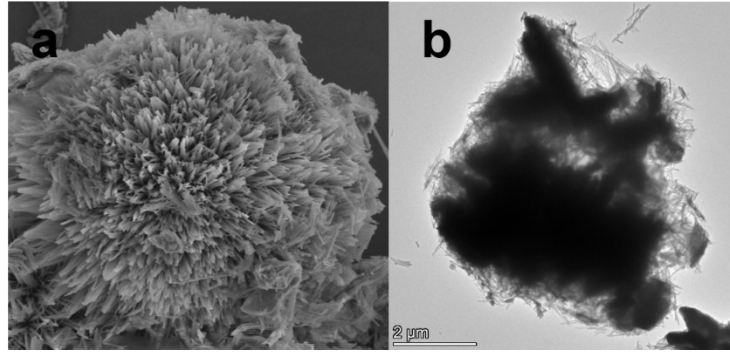


Figure S10. (a) SEM and (b) TEM image of CoP/Mo₂CT_x after the stability test of OER.

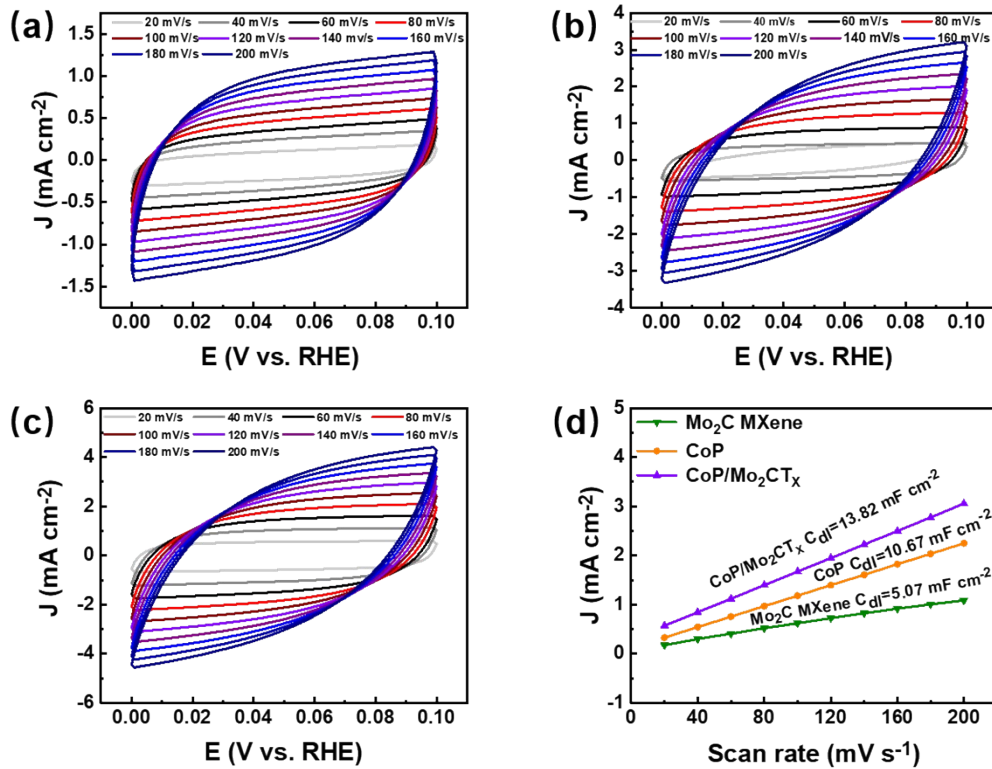


Figure S11. Cyclic voltammograms of (a) Mo₂C MXene, (b) CoP, and (c) CoP/Mo₂CT_x in the region of 0-0.1 V in 1.0 M KOH at various scan rates and (d) the plots of current density as a function of scan rate derived from (a-c), respectively.

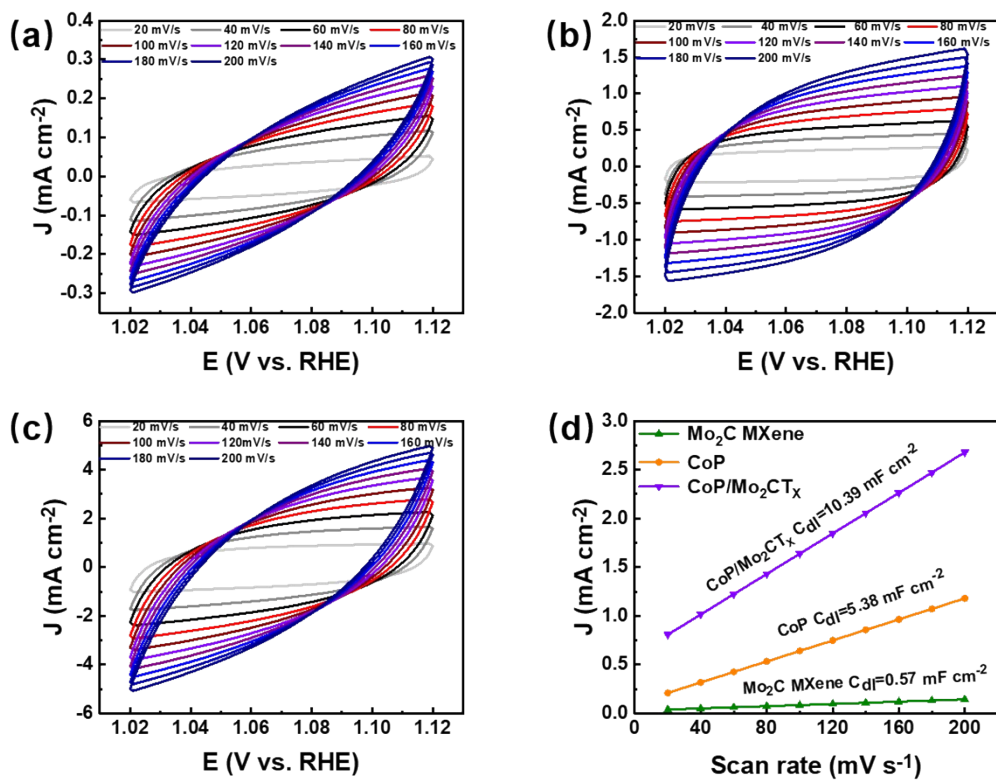


Figure S12. Cyclic voltammograms of (a) Mo₂C MXene, (b) CoP, and (c) CoP/Mo₂CT_x in the region of 1.02–1.12 V in 1.0 M KOH at various scan rates and (d) the plots of current density as a function of scan rate derived from (a–c), respectively.

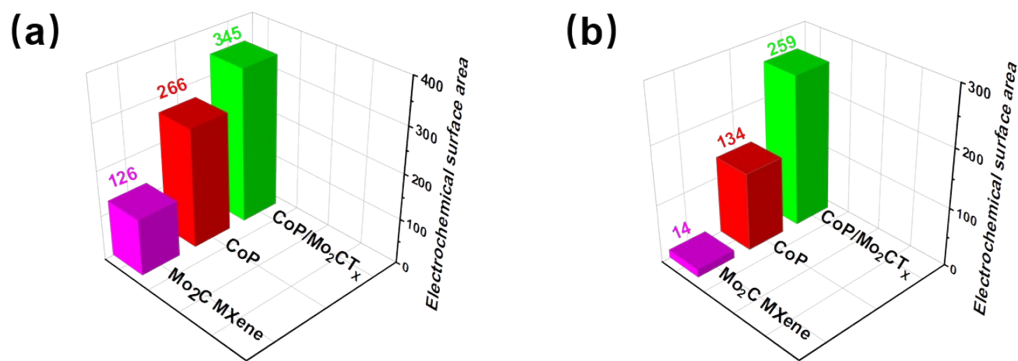


Figure S13. The electrochemically active surface area of different catalysts in HER (a) and OER (b) test.

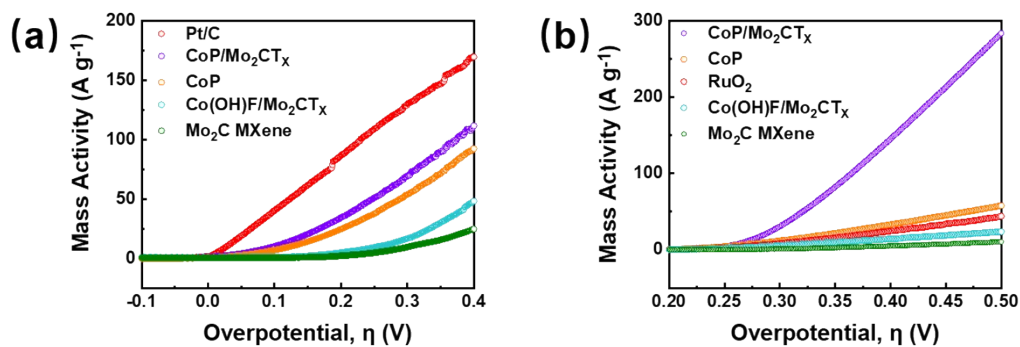


Figure S14. Mass activity for various catalysts in HER (a) and OER (b) test.

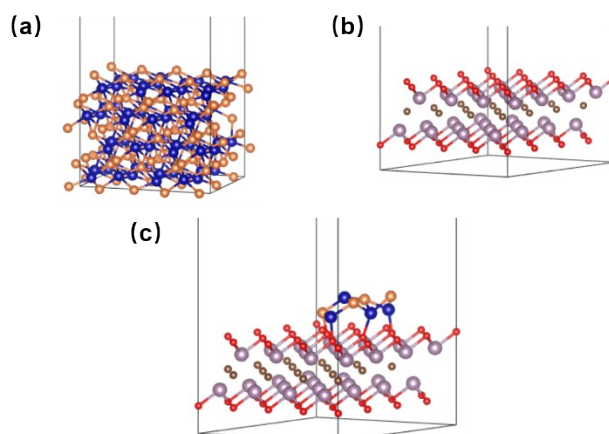


Figure S15. The calculation models of CoP (a), Mo₂C MXene (b), and CoP/Mo₂CT_x (c).

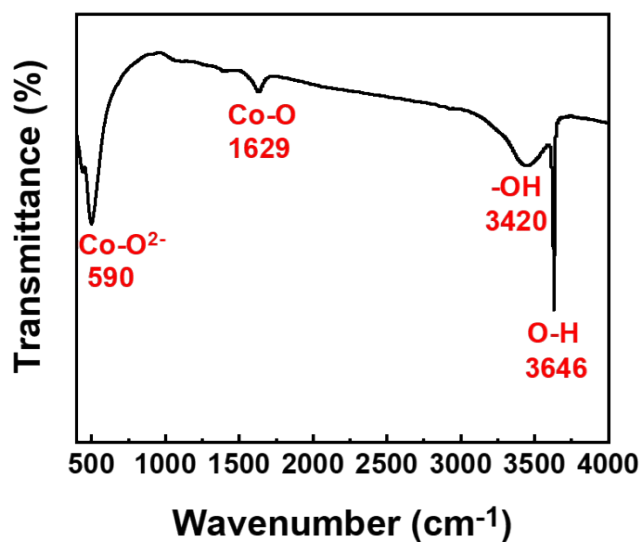


Figure S16. FTIR spectrum of CoP/Mo₂CT_x after OER test.

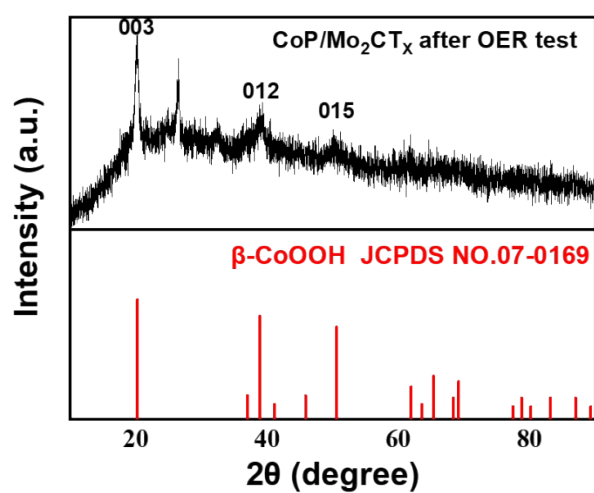


Figure S17. XRD patterns of CoP/Mo₂CT_x after OER test.

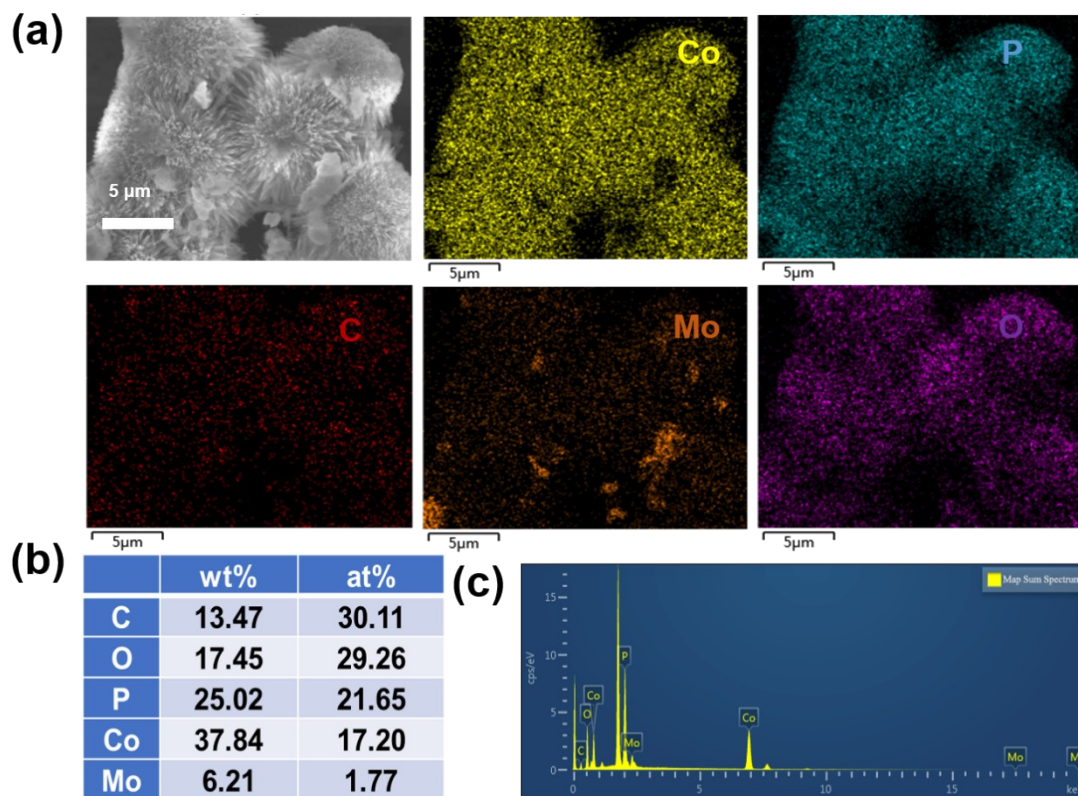


Figure S18. SEM image of CoP/Mo₂CT_x (fresh sample) and corresponding elemental mapping, EDX pattern with elemental composition of CoP/Mo₂CT_x.

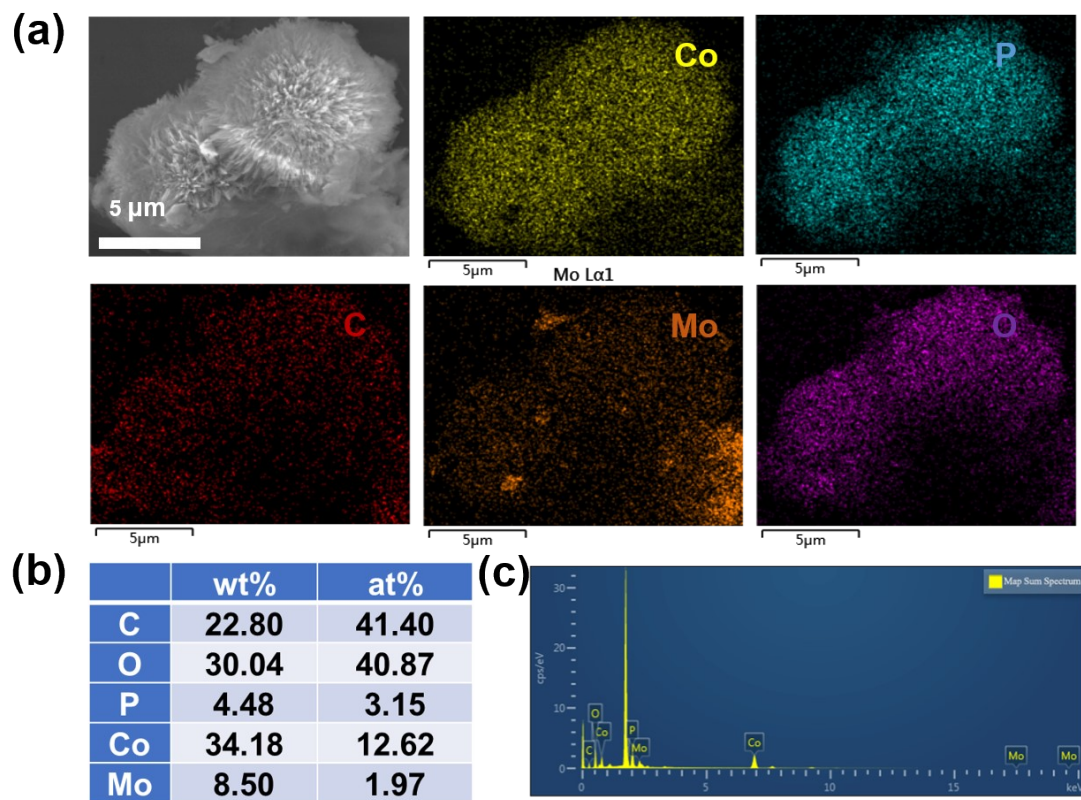


Figure S19. SEM image of CoP/Mo₂CT_x (Post-OER sample) and corresponding elemental mapping, EDX pattern with elemental composition of CoP/Mo₂CT_x.

Table S1. The content of Co, P and Mo elements percentage for all samples, measured by inductively coupled plasma- optical emission spectrometry (ICP-OES).

| Catalyst | Co (wt. %) | P (wt. %) | Mo (wt. %) |
|-------------------------------------|------------|-----------|------------|
| CoP/Mo ₂ CT _x | 31.34 | 25.23 | 17.52 |
| After HER | 34.18 | 18.45 | 16.04 |
| After OER | 38.64 | 3.62 | 16.55 |

Table S2. Comparison of HER performance for non-precious metal electrocatalysts in 1.0 M KOH.

| Electrocatalysts | $\eta@10\text{mA cm}^{-2}$ (mV) | Tafel Slope (mV dec ⁻¹) | Reference |
|--|------------------------------------|--|---|
| CoP/Mo₂CT_x | 78 | 66 | This work |
| CoP/Ti ₃ C ₂ T _x | 116 | 57 | <i>J. Mater. Chem. A</i> , 2019 , <i>7</i> , 27383–27393 |
| CoP@NC | 129 | 58 | <i>ACS Catal.</i> 2017 , <i>7</i> , 3824. |
| Ni _{0.9} Fe _{0.1} PS ₃ @MXene | 196 | NA | <i>Adv. Energy Mater.</i> 2018 , <i>8</i> , 1801127 |
| CoP/CC | 209 | 129 | <i>J. Am. Chem. Soc.</i> 2014 , <i>136</i> , 7587 |
| CoP/NCNHP | 115 | 66 | <i>J. Am. Chem. Soc.</i> 2018 , <i>140</i> , 2610 |
| NC-CNT/CoP | 120 | 73 | <i>J. Mater. Chem. A</i> 2018 , <i>6</i> , 9009 |
| Co-P film/Cu | 94 | 42 | <i>Angew. Chem., Int. Ed.</i> 2015 , <i>54</i> , 625. |
| Co/N-doped carbon | 260 | 91.2 | <i>ACS Nano</i> 2016 , <i>10</i> , 684. |
| CoP NS/C | 110 | 70.9 | <i>Green Chem.</i> 2016 , <i>18</i> , 2287. |
| Co-MoS ₂ /Mo ₂ CT _x | 112 | 82 | <i>Nanoscale</i> 2019 , <i>11</i> , 10992 |
| CoP NFs | 136 | 56.2 | <i>ACS Catal.</i> 2020 , <i>10</i> , 412 |
| CoP@NF | 155 | 96 | <i>Nano Energy</i> 2020 , <i>67</i> , 104174 |
| CoP/CC | 87 | 72 | <i>Appl. Catal. B Environ.</i> 2020 , <i>253</i> , 21 |
| CoP/PC | 76 | NA | <i>Small</i> 2020 , <i>16</i> , 1900550 |
| CoP film | 94 | 42 | <i>Angew. Chem., Int. Ed.</i> 2015 , <i>54</i> , 6251 |

Table S3. Fitting parameters obtained from the EIS data for the HER in 1 M KOH.

| Catalysts | $R_1(\Omega)$ | $R_2(\Omega)$ | $CPE_1-T(F)$ | CPE_1-P | $R_3(\Omega)$ | $CPE_2-T(F)$ | CPE_2-P |
|---|---------------|---------------|--------------|-----------|---------------|--------------|-----------|
| CoP/Mo₂CT_x | 2.567 | 1.347 | 0.11238 | 0.39366 | 3.373 | 0.24052 | 0.77702 |
| CoP | 2.434 | 2.466 | 0.20459 | 0.28379 | 3.479 | 0.24449 | 0.80125 |
| Co(OH)F/Mo₂CT_x | 2.486 | 1.271 | 0.39589 | 0.20214 | 3.841 | 0.23873 | 0.82258 |
| Mo₂C MXene | 3.509 | 5.737 | 0.13236 | 0.47809 | 4.666 | 0.07312 | 0.81123 |

R_1 : electrolyte resistance.

R_2 : charge-transfer resistance.

R_3 : solid-electrolyte interface resistance.

CPE_1 : capacitance generated from the Faradic process, and constant-phase element.

CPE_2 : capacitance arisen from the solid-electrolyte interface process.

Table S4. Comparison of OER performance for non-precious metal electrocatalysts in 1.0 M KOH.

| Electrocatalysts | $\eta@10\text{mA}$ cm^{-2} (mV) | Tafel Slope (mV dec^{-1}) | Reference |
|--|--|--|--|
| CoP/Mo ₂ CT _x | 260 | 51 | This work |
| CoP-MNA/NF | 290 | 65 | <i>Adv. Funct. Mater.</i> 2015 , <i>25</i> , 7337 |
| Co-P film | 345 | 47 | <i>Angew. Chem., Int. Ed.</i> 2015 , <i>54</i> , 6251 |
| CoP NR/C | 320 | 71 | <i>ACS Catal.</i> 2015 , <i>5</i> , 6874 |
| CoP/rGO | 340 | 66 | <i>Chem. Sci.</i> 2016 , <i>7</i> , 1690 |
| CoP/NCNHP | 310 | 70 | <i>J. Am. Chem. Soc.</i> 2018 , <i>140</i> , 2610 |
| Ni _{0.7} Fe _{0.3} PS ₃ @MXene | 282 | 36.5 | <i>Adv. Energy Mater.</i> 2018 , <i>8</i> , 1801127 |
| | 276 | 54 | <i>Nanoscale</i> 2018 , <i>10</i> , 2603 |
| CoP@NPMG | 283 | 53 | <i>Small</i> 2019 , <i>15</i> , 1900550 |
| CoP@PC-750 | 295 | 73 | <i>Nano Energy</i> 2019 , <i>56</i> , 109 |
| CoP/CoO | 337 | 72.1 | <i>Small</i> 2020 , <i>16</i> , 1905075 |
| CoP/TiO _x | 372 | 111.8 | <i>J. Am. Chem. Soc.</i> 2020 , <i>142</i> , 8490 |
| Co ₂ P NRs | 340 | 87 | <i>Adv. Funct. Mater.</i> 2020 , <i>30</i> , 1909618 |
| CoP/CC | 323 | 49.6 | <i>ACS Catal.</i> 2020 , <i>10</i> , 412 |
| CoP NFs | 340 | 66 | <i>Chem. Sci.</i> 2016 , <i>7</i> , 1690. |
| CoP/Graphene | 330 | 40 | <i>ACS Appl. Mater. Interfaces</i> 2015 , <i>7</i> , 28412. |
| CoP/CNT | | | |

Table S5. Fitting parameters obtained from the EIS data for the OER in 1 M KOH.

| Catalysts | $R_1(\Omega)$ | $R_2(\Omega)$ | $CPE_1-T(F)$ | CPE_1-P | $R_3(\Omega)$ | $CPE_2-T(F)$ | CPE_2-P |
|---|---------------|---------------|--------------|-----------|---------------|--------------|-----------|
| CoP/Mo₂CT_x | 2.674 | 1.091 | 0.01291 | 0.53243 | 3.389 | 0.046454 | 0.70913 |
| CoP | 2.475 | 1.888 | 0.16482 | 0.33264 | 3.452 | 0.25667 | 0.81997 |
| Co(OH)F/Mo₂CT_x | 2.494 | 1.696 | 0.12766 | 0.36013 | 3.514 | 0.26314 | 0.82463 |
| Mo₂C MXene | 2.403 | 1.873 | 0.24933 | 0.19699 | 3.815 | 0.05575 | 0.74074 |

R_1 : electrolyte resistance.

R_2 : charge-transfer resistance.

R_3 : solid-electrolyte interface resistance.

CPE_1 : capacitance generated from the Faradic process, and constant-phase element.

CPE_2 : capacitance arisen from the solid-electrolyte interface process.

Table S6. Comparison of the water splitting cell voltage of CoP/Mo₂CT_x with recently reported bifunctional electrocatalysts in alkaline medium.

| Electrocatalyst | Potential (V) at 10 mA cm ⁻² | Reference |
|-------------------------------------|--|--|
| CoP/Mo ₂ CT _x | 1.56 | This work |
| NiCoP/rGO | 1.59 | <i>Adv. Funct. Mater.</i> 2016 , 26, 6785. |
| Co-P film | 1.65 | <i>Angew. Chem. Int. Ed.</i> 2015 , 54, 6251 |
| CoP-MNA | 1.62 | <i>Adv. Funct. Mater.</i> 2015 , 25, 7337 |
| CoP NR | 1.587 | <i>ACS Catal.</i> 2015 , 5, 6874 |
| NiCoP/Ti | 1.64 | <i>Adv. Mater. Interfaces</i> 2016 , 3, 1500454 |
| CoP nanosheets | 1.54 | <i>Green Chem.</i> 2016 , 18, 2287 |
| CoP/GO | 1.7 | <i>Chem. Sci.</i> 2016 , 7, 1690 |
| CoP/CC | 1.61 | <i>ChemSusChem</i> 2016 , 9, 472 |
| Fe-CoP/Ti | 1.60 | <i>Adv. Mater.</i> 2017 , 29, 1602441 |
| CoP NA/CC | 1.65 | <i>ChemElectroChem</i> 2017 , 4, 1840 |
| Ni-Co-P HNBS | 1.62 | <i>Energy Environ. Sci.</i> 2018 , 11, 872 |
| S:CoP@NF | 1.617 | <i>Nano Energy</i> 2018 , 53, 286 |
| CoP-400 | 1.65 | <i>Adv. Energy Mater.</i> 2018 , 8, 1802445 |
| CoP@a-CoOx | 1.66 | <i>Adv. Sci.</i> 2018 , 5, 1800514 |
| CoP/NCNHP | 1.64 | <i>J. Am. Chem. Soc.</i> 2018 , 140, 2610 |